Persistence Mapping Using EUV Solar Imager Data

B. J. Thompson

NASA Goddard Space Flight Center, Code 671, Greenbelt, MD 20771, USA

barbara.j.thompson@nasa.gov

and

C. A. Young

NASA Goddard Space Flight Center, Code 670, Greenbelt, MD 20771, USA

Received 15 July 2015; accepted _____

ABSTRACT

We describe a simple image processing technique that is useful for the visualization and depiction of gradually evolving or intermittent structures in solar physics extreme-ultraviolet imagery. The technique, which we call "Persistence Mapping," allows the user to isolate extreme values in a data set, and is particularly useful for the problem of capturing phenomena that are evolving in both space and time. While integration or "time lapse" imaging uses the full sample (of size N), Persistence Mapping rejects (N-1)/N of the data set and identifies the most relevant 1/N values using the following rule: if a pixel reaches an extreme value, it retains that value until that value is exceeded. The simplest examples isolate minima and maxima, but any quantile or statistic can be used. This paper demonstrates how the technique has been used to extract the dynamics in long-term evolution of comet tails, erupting material, and EUV dimming regions.

Subject headings:

1. Introduction

Many important solar phenomena have dynamic natures that make them difficult to identify and capture. In particular, features that evolve in both space and time require processing techniques that can extract the key physical attributes from increasingly large data sets. We describe a processing technique that is simple to implement, yet captures several important aspects of spatial/temporal evolution. This technique, called "Persistence Mapping," can be used on its own, or it can provide important pre-processing information for more sophisticated algorithms.

For a data set consisting of N images with emissions values *I(x,y,t)*, the Persistence Map P_n is a function of several arguments, namely emission, location and time:

$$P_n(x, y, t_n) = Q(I(x, y, t \leqslant t_n))$$

where x, y and t are the spatial and temporal coordinates, $t_0 < t_n \leqslant t_N$ are the image sampling times, and Q is the selection function. The most common (and simplest) forms of Q are minimum and maximum values, but any quantile or statistic can be used. For a maximum value Persistence Map (such as the ones shown in Figures 3 and 4), $P_n(x,y,t_n)$ represents the maximum value of the location *(x,y)* evaluated for the time range t_0 (first image) to t_n (current image). Similarly, minimum value Persistence Maps are shown in Figures 7, 9, 10, and 11.

While Persistence Maps can capture the evolution of a feature over time, the technique is different from averaging or "time-lapse" integration in that it chooses a single data value to represent location *(x,y)* for all times up to t_n. If the desired feature or phenomenon is rare or intermittent, averaging or integrating a large data set can significantly decrease the signal relative to the background. The distinction is particularly important when the number of images N becomes large compared to the number of times the feature is observed

at a given location; if the feature is only present at location *(x,y)* for one image, Persistence Mapping discards the information from the other N-1 images.

A persistence function was introduced by Fredkin et al. (1985) as a means of characterizing noise in ion-channel activity. Their persistence function is the probability that the current will be at a particular level at a particular point in time, based on the past variations in the current. The examples we show in this paper are much more simple, and are adapted more for imager data.

Of course, the degree of success yielded by the Persistence Mapping technique depends on the ability to optimize the mapping function Q for a particular feature or phenomenon; not all solar features consistently exhibit clearly identifiable extremes such as minima and maxima. In the next section we present several examples of solar phenomena that fit this criterion, and demonstrate how Persistence Mapping can rapidly distill key characteristics from large data sets.

2. Implementation Examples

2.1. Maximum value Persistence Mapping of a slowly evolving feature: Comet Lovejoy

Our first example uses data from the Atmospheric Imaging Assembly (Lemen et al. (2012); Boerner et al. (2012)) on the Solar Dynamics Observatory (Pesnell et al. (2012)). The Comet Lovejoy transited the solar corona December 15 and 16, 2011, and was well observed by investigations on several solar missions. Of particular interest is the physics behind the formation of the EUV tail (*c.f.* Bryans & Pesnell (2012); Schrijver et al. (2012); McCauley et al. (2013); Downs et al. (2013); Raymond et al. (2014)).

Comet Lovejoy is a particularly powerful demonstration of the persistence technique

because the time history of the comet's interaction with the corona is key to understanding its behavior. McCauley et al. (2013), Downs et al. (2013) and Raymond et al. (2014) demonstrated how the behavior of the tail, or coma, present a unique opportunity to diagnose the magnetic field of the local corona. To study long-term behavior of the coma, Raymond et al. (2014) averaged multiple images over the transit of Lovejoy through the corona; we will demonstrate how persistence mapping can be applied instead.

Figures 1 and 2 show the late stages of the inner coronal transit of the Comet Lovejoy. The coma shows clear evolution in time, with an apparent "kink" shape developing around 00:43:48 UT on 2011 December 16 (the kink is most apparent in Figure 2 panels c and d). Figure 3 shows the sequence processed with the persistence technique, where Q is the maximum value evaluated from t_0 = 2011-Dec-16 at 00:40 UT to the time of each particular image (the top panel of Figure 3 is the original image shown for comparison).

Figure 4 shows subframes of the persistence maps to elucidate the paths of emission, tracing out elongated features. The persistence technique allows the user to clearly identify the flow direction of the comet's tail emission. The coma consists of individual cores of emitting plasma, originating at the point where the comet nucleus intersects the corona, but then spreading along the connected field lines. Note that the "kink" in the tail, that is most evident in panels b) and c) in Figure 2, corresponds to a divergence in flow direction of the emitting plasma in the corresponding panels in Figure 4.

It is important to distinguish persistence methods from "integration" or "averaging," which are also common ways of combining information from a large number of images. The bottom panel in Figure 3 shows the average value per pixel over the sample period. Rather than clearly isolating the desired bright features, the frames with the comet emission simply contribute to the average value of 97 images. The emission is rapidly evolving early in the comet's transit, meaning that the pixels that exhibit the coma emission is averaged with

99% of the images showing no coma emission. Later in the transit, where the emission lasts for several minutes, the coma is somewhat visible, but not nearly as visible as in the persistence map in the center panel. The persistence technique isolates a single value and excludes the other 96, averaging produces a less optimal result. Of course, each situation requires a careful consideration of which technique will work best; there are cases where averaging and integration will produce a more ideal result than persistence, such as a collection of individual images with low signal. Persistence may tend to pick out the noise in low-signal images, making it a poor choice of processing method.

2.2. Minimum value Persistence Mapping of a slowly evolving feature: Coronal dimming

Our second example involves a coronal dimming feature that evolves slowly with time. Coronal dimmings are known to be good indicators of the site of evacuated material, and possible open field lines, during coronal mass ejections (*e.g.* Rust & Hildner (1976); Webb et al. (1978); Rust (1983); Sterling & Hudson (1997); Gopalswamy & Hanaoka (1998); Thompson et al. (2000); Reinard & Biesecker (2008); Reinard & Biesecker (2009)). They are typically easy to identify, in that they occur in areas of relatively quiet, slowly-evolving Sun and usually persist for at least one hour.

However, dimmings can extend far from the erupting region, and are sometimes patchy in appearance, with some areas reaching their lowest emission value long before separate but apparently related areas. An important aspect of dimming studies is identifying the full dimming area, and not simply the areas that exhibit a decrease at a given time. We use the dimming/flare/CME event of 2010 November 30 as an example of a "challenging" dimming region.

Figure 5 shows a series of combined wavelength (Red layer = 211Å, Green = 193Å, Blue=171Å) images sampled from 17:05 UT on 2010 November 30 through 2:00 UT 2010 December 1. The first frame, 17:05 UT, is a "pre-event" image, as there is no evidence of the flare and dimming until several minutes later. In Figure 5, we identify several areas that exhibit dimming, including

A: a pre-existing dark region (perhaps coronal hole) that becomes even darker

B: an area that darkens soon after the flare begins and persists for many hours

C: an area that darkens soon after the flare begins, but is later obscured by flare loops

D: an area that darkens soon after the flare but then "recovers" within a few hours

E: a darkened area that appears relatively late in the timeline, after areas C and D have mostly disappeared

Given the range of times and locations of the many dimming areas, how can one be certain that all of the dimmings are appropriately captured? The traditional method is to perform "base difference" images (Figure 6), where a pre-event image (17:00 UT) is subtracted from each image to highlight only the areas that changed. However, because the different dimming regions grow and recover on different timescales, it is a challenge to combine images from multiple times to capture the full combined extent of all of the dimming regions. Additionally, a well-known property of taking base or running differences of images is the addition of noise (Hamming (1997)).

This event is an excellent candidate for the persistence technique because persistence retains the lowest value over the specified timescale, so even if an image starts to "recover" during the sequence it does not impact subsequent images. Figure 7 shows the same images as Figures 5 and 6, processed with the persistence technique where Q = minimum value for each individual wavelength from $t_0 < t_n \leqslant t_N$ and t_0 = 2010 November 30 at 17:00 UT.

There are several things to note about Figure 7 and the associated movie. First, the

flare does not appear *at all* in the persistence images and movie, because the technique disregards any pixels that do not decrease in emission. The movie shows dimming regions appearing in the complete absence of any associated flaring activity. (Similarly, a user who is interested in the flare could apply maximum persistence and remove all evidence of dimming.) Second, it is clear from the persistence images that areas C) and D) are in fact one region that evolves inhomogeneously, and that area A) is the only one that is completely disconnected from the other four. This information can also be derived from examination of the base difference images, but the last panel of Figure 7 illustrates how quickly and simply a full dimming map can result from persistence mapping. (Of course, a user who is interested measuring emission from the flare without "contamination" from the dimmings may consider applying Q=maximum to isolate the flare loops).

2.3. Minimum value Persistence Mapping of an intermittent feature: Erupting prominence

Our final example details a rapidly evolving phenomenon: falling prominence material viewed in absorption against the bright corona. Figure 8 clearly shows a large prominence on 2011 June 7 that erupts, but a large fraction of the erupting material falls back to the Sun (Reale et al. (2013); Gilbert et al. (2013)). The challenge of measuring and analyzing the falling material is complicated by the fact that the overall shape is continually evolving, and individual features are not easily distinguished within the large moving mass.

In Figure 9 we apply the Q=minimum technique for the 2011 June 7 eruption as seen by AIA in 193Å, sampling with the maximum image cadence (12 seconds) with Q=minimum and t_0=2011 June 7 05:00:07 UT. Figure 10 shows a close-up of a portion of the image, highlighting the variation in trajectories. The persistence map is able to highlight the various trajectories exhibited by different parts of the prominence. However,

the prominence eventually traverses a large fraction of the visible area, and it becomes difficult to distinguish one trajectory from another.

Figure 11 illustrates how the timing and cadence can be chosen to optimize the resultant map. In particular, there is the challenge of determining which trajectories in the SDO images correspond to the trajectories as observed from the STEREO-A EUVI viewpoint, located at .96 AU, 94 degrees from Earth. A 12-second SDO cadence is not ideal because the location of the prominence did change significantly from one frame to the next. Additionally, choosing a long sequence of images is not optimal when multiple trajectories overlap; by fine-tuning t_0 and the sampling time we can isolate individual trajectories more clearly.

In Figure 11 we apply the Q=minimum technique, but instead of sampling with the maximum SDO image cadence (12 seconds), we sample every two minutes up to 11:00 UT, with $t_0 < t_n \leqslant t_N$ where n = multiples of 10 and t_0 = 05:00:07 UT. These maps were used to determine the 3-D trajectories of impacting blobs reported in Gilbert et al. (2013). The temporal evolution of the prominence motion is revealed by the resampling, or "strobing" of images. Although there were many separate trajectories, we projected the locations of a piece of prominence as viewed by SDO to their corresponding lines of sight in the EUVI map. When we required the material in the EUVI map to match the timing and lines of sight of the material in the AIA map, unique trajectories were able to be identified and measured.

3. Discussion and Conclusions

This technique, while being extremely simple to implement, provides a concise and elegant way to capture the evolution of various solar phenomena. As shown in the examples,

the choice of persistence function Q and sample timing can be tailored to produce a desired result. The persistence technique differs from "long exposure" or "integration" because the latter techniques do not identify and exclude "unwanted" data points. While an integration of 100 images results in 100 values counting equally, the persistence technique completely exclude 99 of the images, retaining only the one value that satisfies the Q criterion. For phenomena evolving in both time and space, persistence maps are more distinct and it is easier to identify individual features.

Of course, the persistence maps become more useful with increasing number of images. If there are only a few images that are relevant, other techniques may more effectively produce the desired result. It is also important to understand the limitations of the maps early in the sequence $t_0 < t_n \leqslant t_N$; the number of pixels that change in a map is on average 1/n, so for low values of n a large fraction of the pixels will change, while for the 100th image there is only 1% chance of change.

Persistence maps can also be implemented as a "pre-processing step" for more sophisticated analysis; the maps can highlight exactly which subset of the observing area exhibits a given phenomenon, allowing the user to isolate the regions on which to focus.

As with most methods, artifacts can be misleading. For most of the maps in this paper, the features in the map appear to last indefinitely. From the map alone, one usually cannot tell if the feature lasted only one frame or one hundred frames. Therefore, it is recommended that the maps always be viewed in concert with the "normal" images, so the user can view both the development and the decay of a transient phenomenon.

The authors are interested in identifying new applications for the persistence mapping technique. We encourage the reader to check http://sipwork.org/persistence for updated examples and discussion.

The authors would like to thank Dean Pesnell, Paul Bryans, Michael Chesnes, Mark Cheung, Cooper Downs, Wei Liu, and Leila Mays for discussion and assistance in developing this technique.

REFERENCES

Boerner, P., Edwards, C., Lemen, J., et al. 2012, Sol. Phys., 275, 41

Bryans, P., & Pesnell, W. D. 2012, ApJ, 760, 18

Downs, C., Linker, J. A., Mikić, Z., et al. 2013, Science, 340, 1196

Fredkin, D. R., Rice, J. A., Colquhoun, D., Gibb, A. J. 1995, *Philosophical Transactions: Biological Sciences*, 350, 334, 353

Gilbert, H. R., Inglis, A. R., Mays, M. L., Ofman, L., Thompson, B. J., Young, C. A. 2013, ApJ, 776, L12

Gopalswamy, N., & Hanaoka, Y. 1998, ApJ, 498, L179

Hamming, R. W. 1997, "Digital Filters," Prentice-Hall, ISBN # 9780486650883

Lemen, J. R., Title, A. M., Akin, D. J., et al. 2012, Sol. Phys., 275, 17

McCauley, P. I., Saar, S. H., Raymond, J. C., Ko, Y.-K., & Saint-Hilaire, P. 2013, ApJ, 768, 161

Pesnell, W. D., Thompson, B. J., & Chamberlin, P. C. 2012, Sol. Phys., 275, 3

Raymond, J. C., McCauley, P. I., Cranmer, S. R., & Downs, C. 2014, ApJ, 788, 152

Reale, F., Orlando, S., Testa, P., et al. 2013, Science, 341, 251

Reinard, A. A., & Biesecker, D. A. 2008, ApJ, 674, 576

Reinard, A. A., & Biesecker, D. A. 2009, ApJ, 705, 914

Rust, D. M., & Hildner, E. 1976, Sol. Phys., 48, 381

Rust, D. M. 1983, Space Sci. Rev., 34, 21

Schrijver, C. J., Brown, J. C., Battams, K., et al. 2012, Science, 335, 324

Sterling, A. C., & Hudson, H. S. 1997, ApJ, 491, L55

Thompson, B. J., Cliver, E. W., Nitta, N., Delannée, C., & Delaboudinière, J.-P. 2000, Geophys. Res. Lett., 27, 1431

Webb, D. F., Nolte, J. T., Solodyna, C. V., & McIntosh, P. S. 1978, Sol. Phys., 58, 389

This manuscript was prepared with the AAS LaTeX macros v5.2.

Fig. 1.— Comet Lovejoy as seen in an AIA 171Å image taken 16 December 2011 at 00:43:00 UT. Image has been enhanced radially and with wavelet processing. The northwest limb of the Sun is visible in the lower left corner. The animation of the comet's passage from 16 December 2011 00:40:00 to 01:00:00 UT is included in the electronic version of this paper.

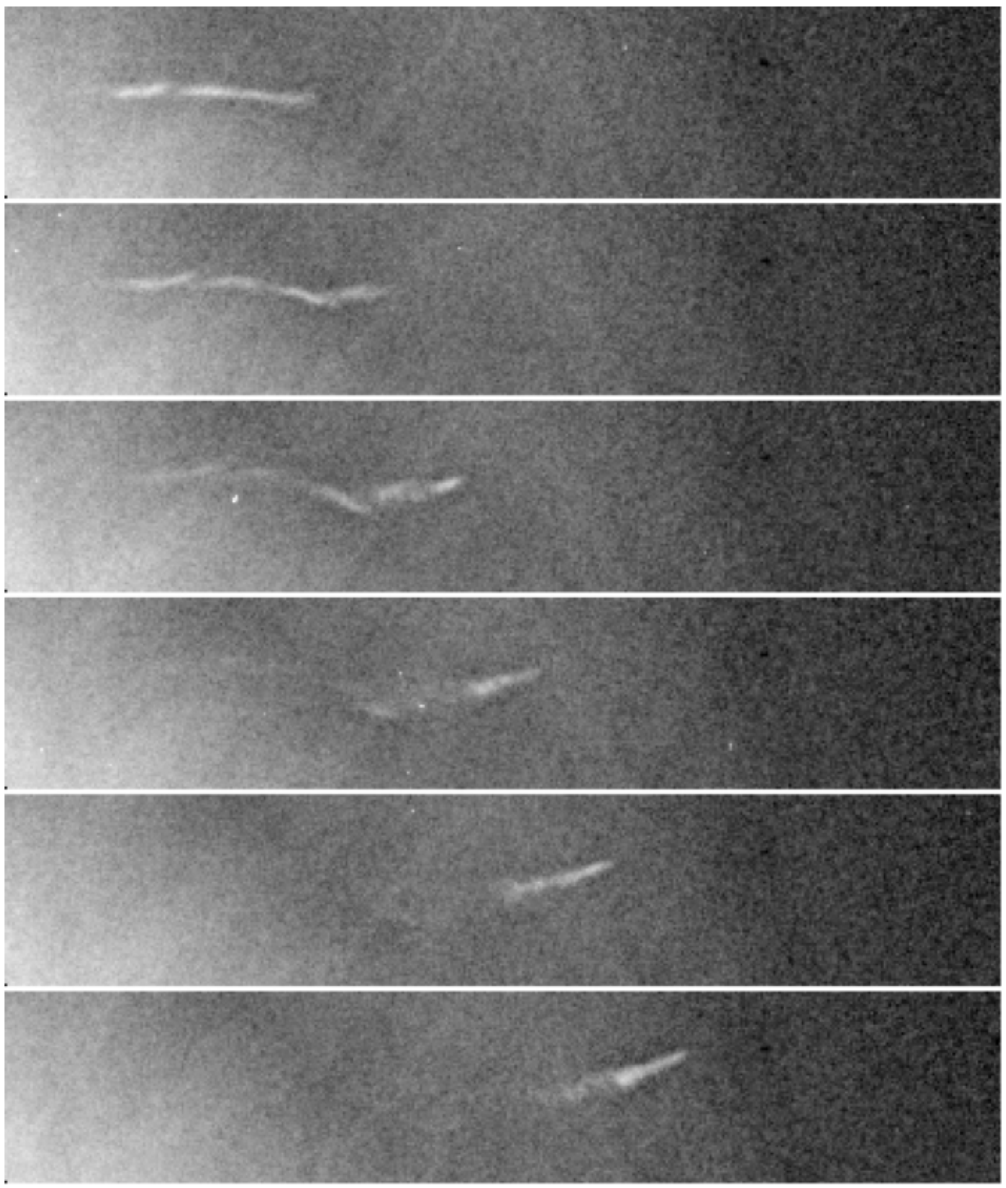

Fig. 2.— AIA 171Å images sampled at 24 seconds (AIA cadence is 12 seconds) from top to bottom: 16 December 2011 at 00:43:00 UT (a closeup of Figure 1), 00:43:24 UT, 00:43:48 UT, 00:44:12 UT, 00:44:36 UT and 00:45:00 UT. Images have been enhanced radially and with wavelet processing.

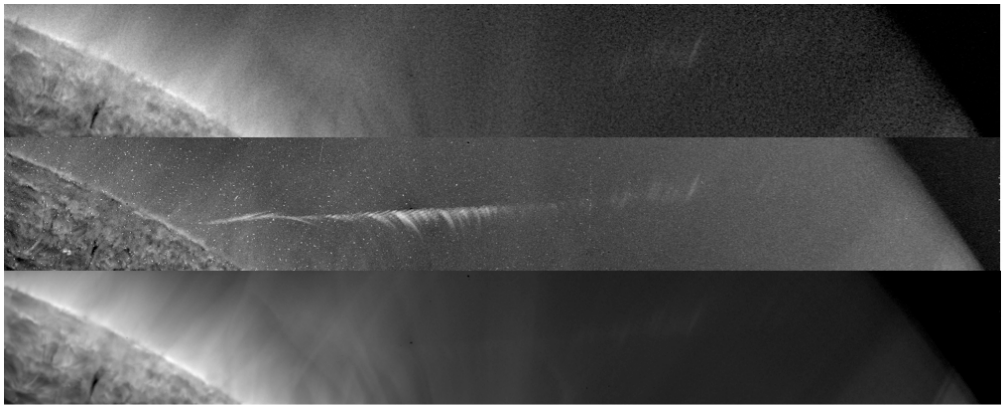

Fig. 3.— Top: AIA 171Å image from 16 December 2011 at 00:57:01 UT. Center: Persistence image at 00:57:00 UT, assembled from 81 AIA 171Å images sampled at a 12-second cadence starting at 00:40:11 UT. Bottom: For comparison, the average pixel value for the entire sequence 00:40 - 01:00 UT is shown. The earliest locations of the coma are not at all visible in the average image, because it is rapidly evolving and the bright features have little impact on the average. The longer-lasting emission later in the transit is faintly visible, but not as clear as in the persistence map. All images were enhanced radially and with wavelet processing. The animation of the top and center panels from this figure for the times 16 December 2011 00:40:00 to 01:00:00 UT is included in the electronic version of this paper.

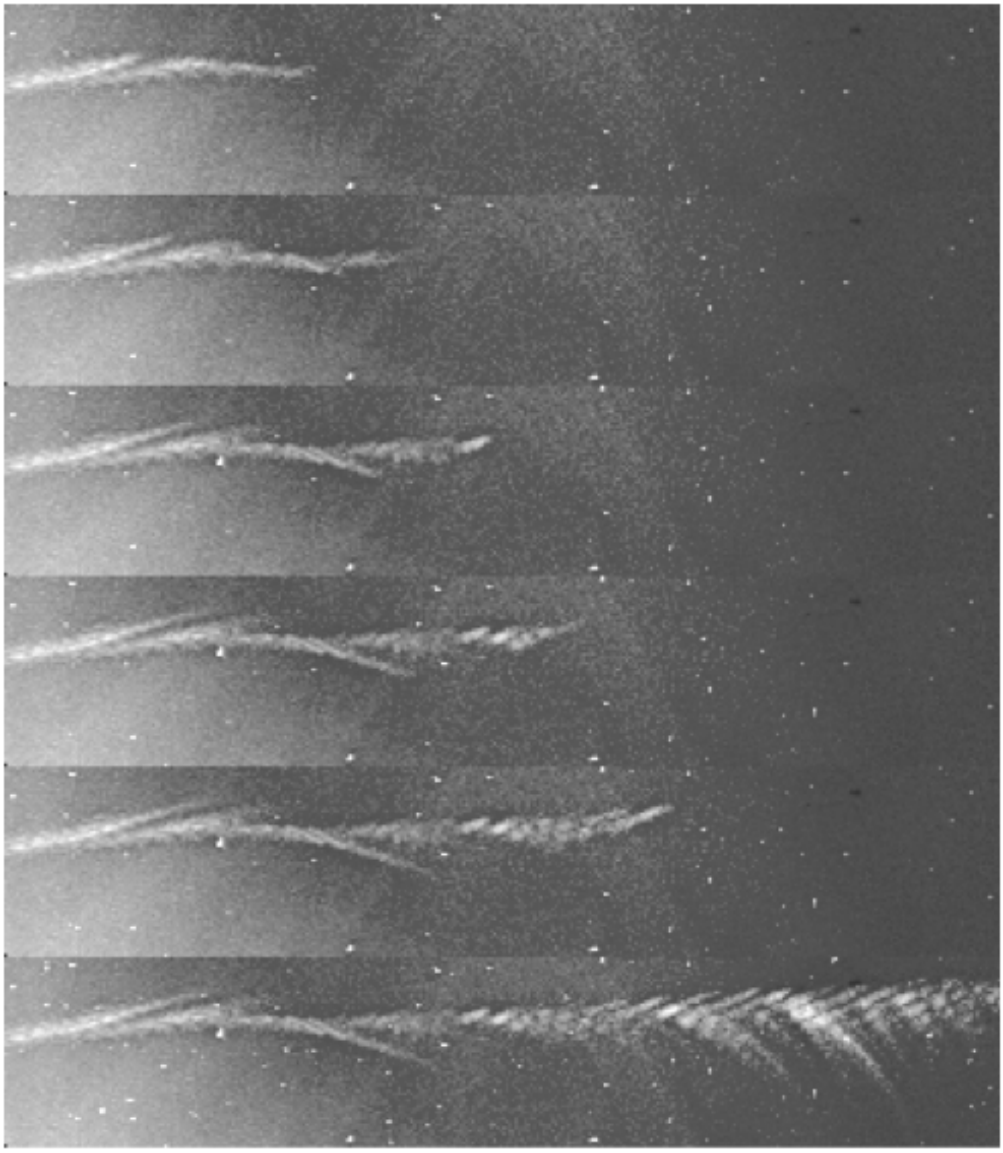

Fig. 4.— The top five frames show the images from Figure 2 (corresponding to times 00:43:00 UT, 00:43:24 UT, 00:43:48 UT, 00:44:12 UT, 00:44:36 UT) processed using the persistence technique, where Q is the maximum value function for $t_0 < t_n \leqslant t_N$ and t_0 = 00:40:11 UT. The top 5 panels were assembled using AIA 171Å images sampled at a 12-second cadence starting at 00:40:11 UT, up to the time corresponding to the panel. The sixth panel shows the persistence values evaluated at 00:49:00 UT to show the later progress of the comet. The lateral striation effect is due to the sampling period of the images.

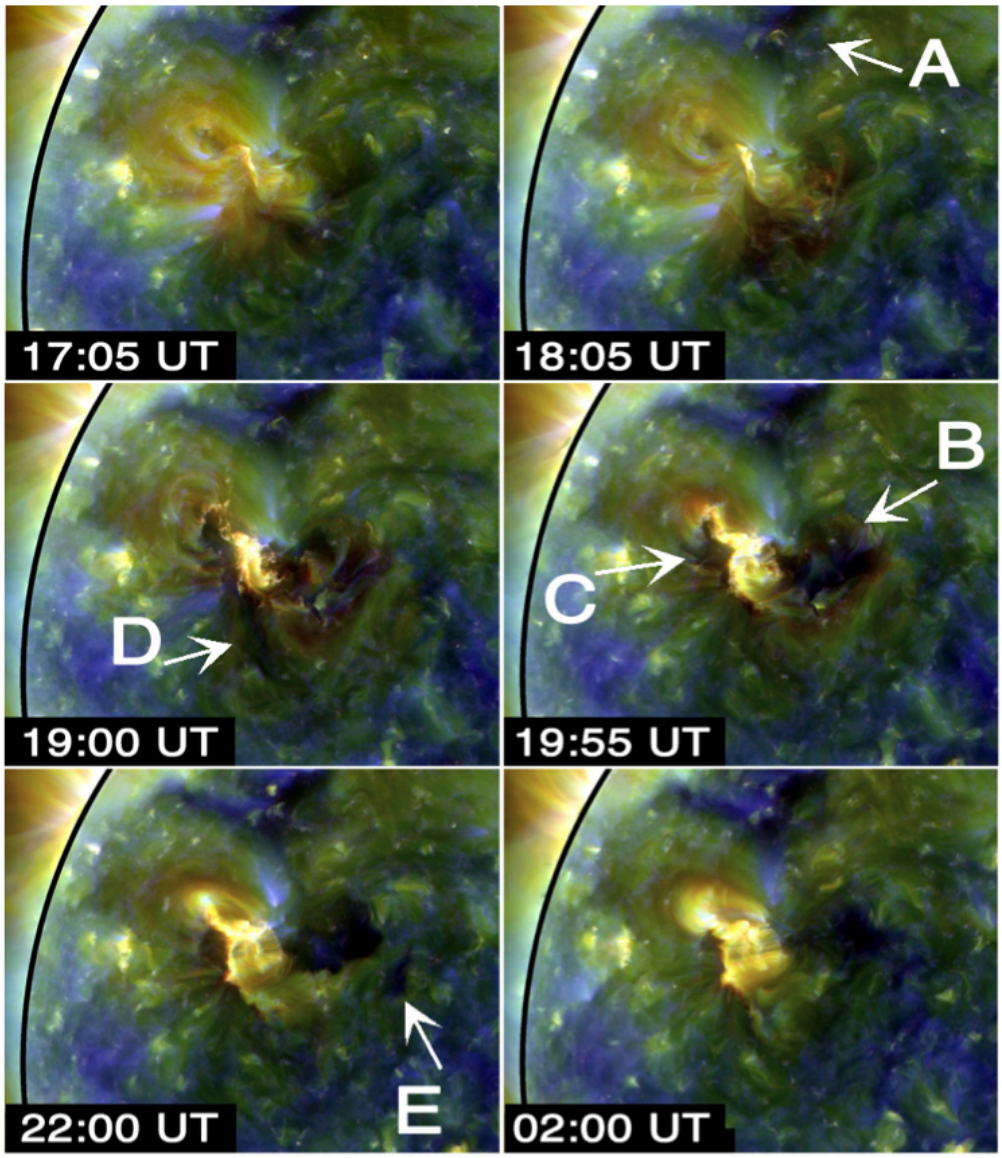

Fig. 5.— AIA combined wavelength images (Red=211Å, Green=193Å, Blue=171Å) for the dimming/flare/CME event on 2010 November 30 17:05 UT, 18:05 UT, 19:00 UT, 19:55 UT, 22:00 UT, (December 1) 02:00 UT. Regions A - E all exhibited dimming at some point during the event, but the much of the early dimming has disappeared by the time region 'E" appears. The animation of this figure from 2010 November 30 17:00 - 2010 December 1 02:55 UT is included in the electronic version of this paper.

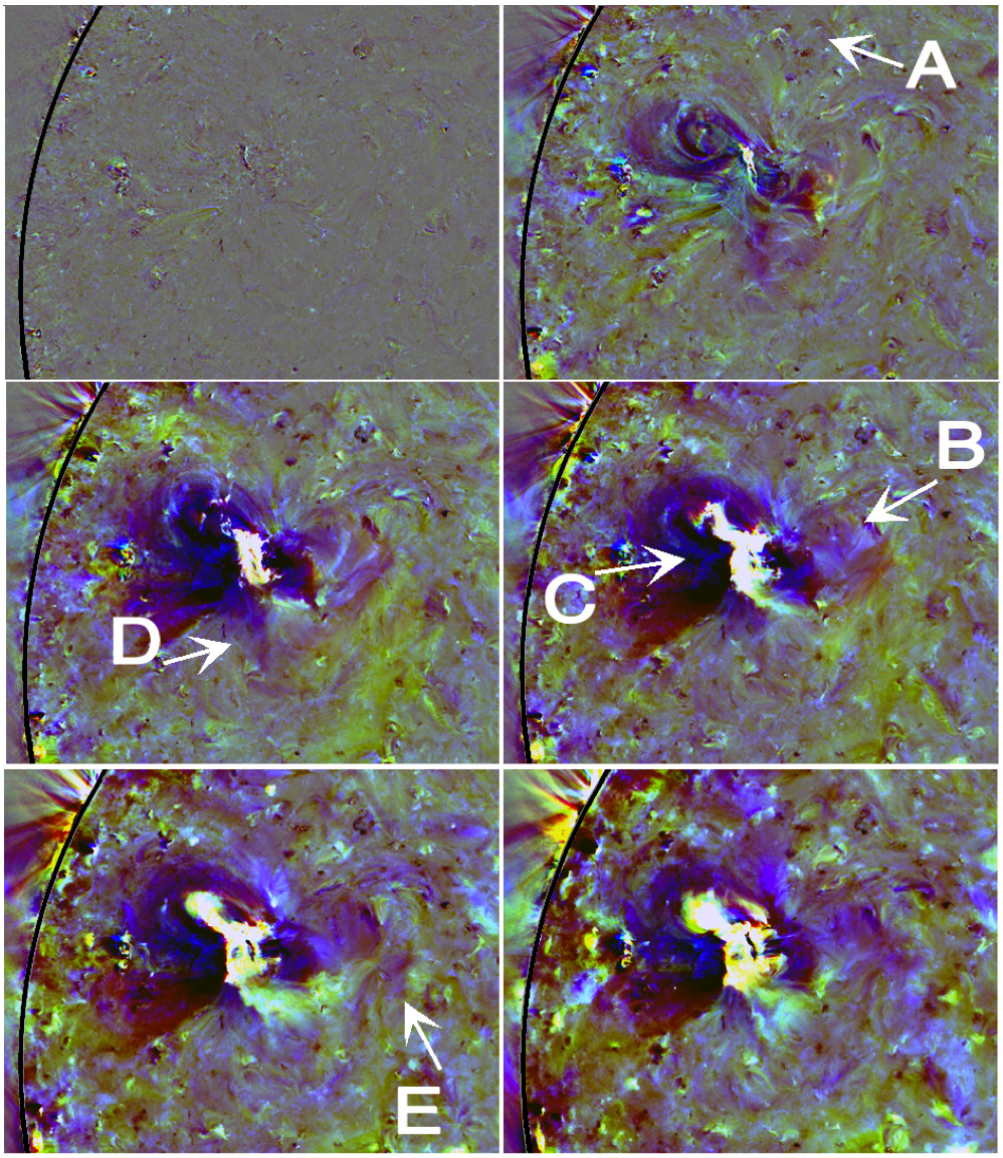

Fig. 6.— AIA combined wavelength images from Figure 5 with "base images" at 17:00 UT subtracted off (i.e. Red layer is 211Å images with the 17:00 211Å image subtracted from it, Green is 193Å images with the 17:00 193Å image subtracted from it, and same for Blue and 171Å). The animation of this figure from 2010 November 30 17:00 - 2010 December 1 02:55 UT is included in the electronic version of this paper.

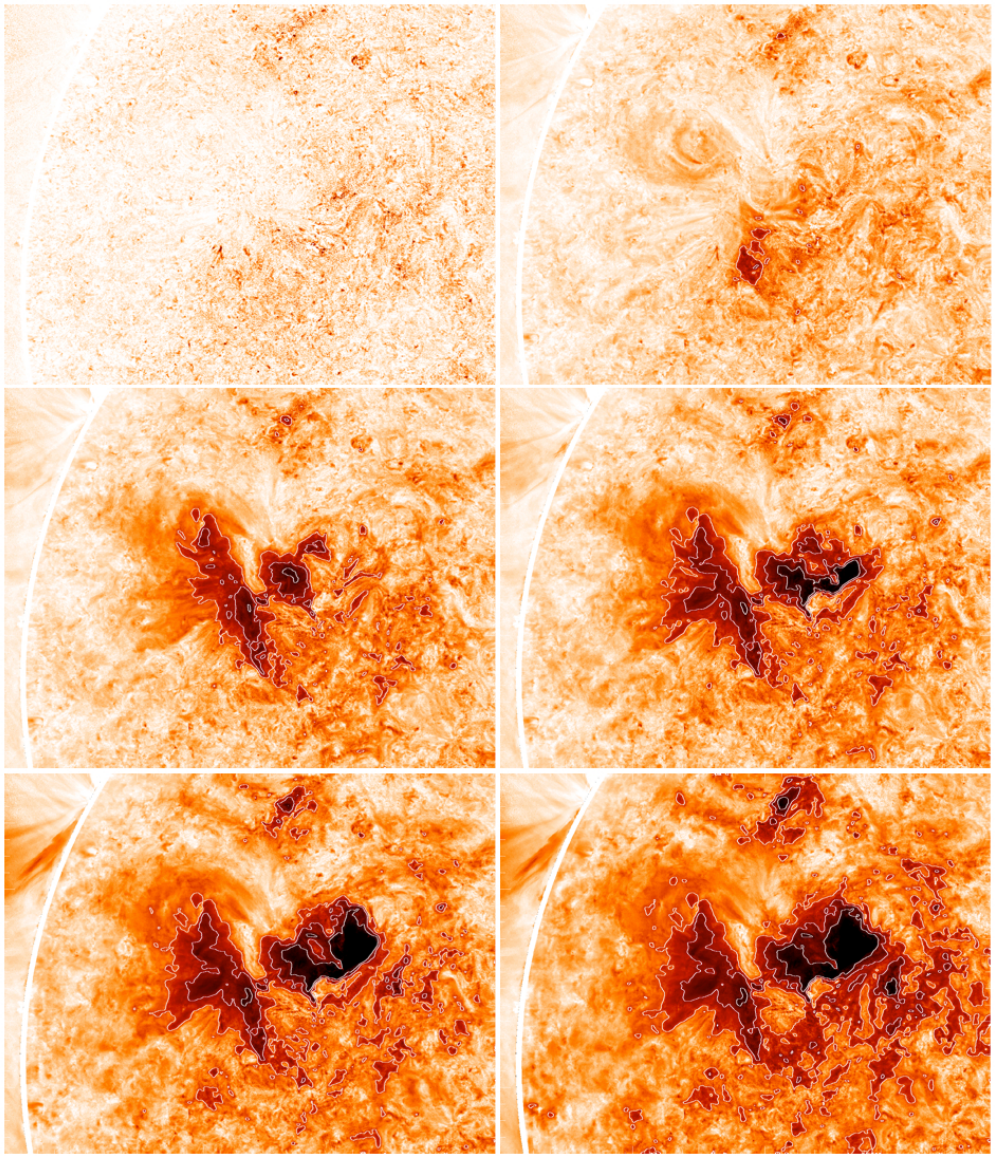

Fig. 7.— AIA combined wavelength images processed with the persistence technique. Each wavelength was processed independently using the persistence technique, with Q = minimum value per wavelength from $t_0 < t_n \leqslant t_N$ and t_0 = 2010 November 30 at 17:00 UT. Contours outline intensity decrease weighted across the three wavelengths (171Å, 193Å and 211Å). The animation of this figure from 2010 November 30 17:00 - 2010 December 1 02:55 UT is included in the electronic version of this paper.

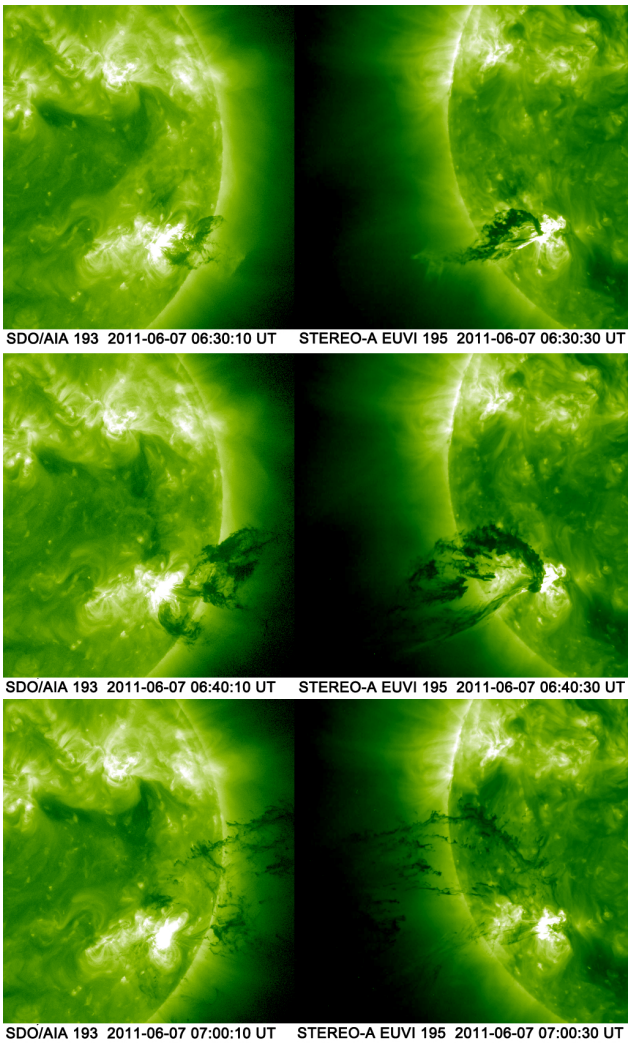

Fig. 8.— Erupting prominence observed from two viewpoints: SDO 193Å (left panels) and STEREO-A EUVI 195Å (right panels). Note that the color table for SDO 193Å has been altered to match the EUVI color table to facilitate comparison. The animation of this figure from 2011 June 7 05:40 - 11:55 UT is included in the electronic version of this paper.

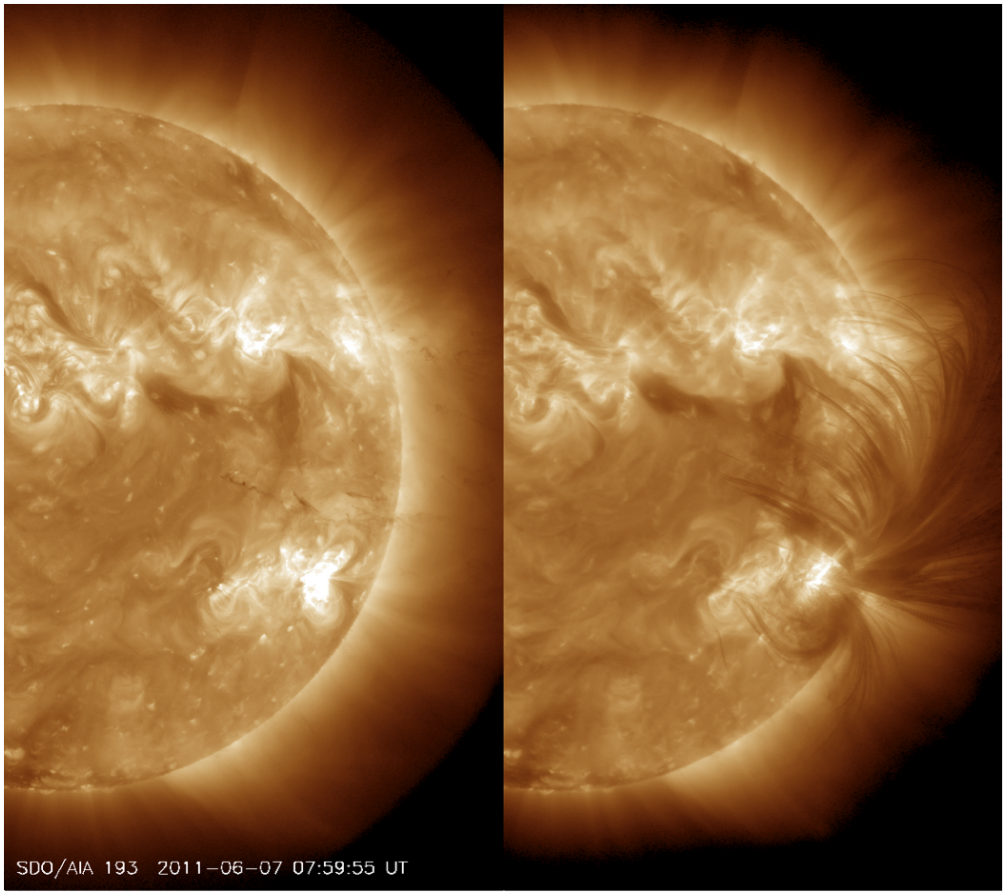

Fig. 9.— Persistence map evaluated at 2011 June 7 07:59:55 for the SDO 193Å images with Q = minimum value per wavelength from $t_0 < t_n \leqslant t_N$ and t_0 = 2011 June 7 at 05:40 UT. The animation of this figure from 2011 June 7 05:40 - 08:00 UT is included in the electronic version of this paper.

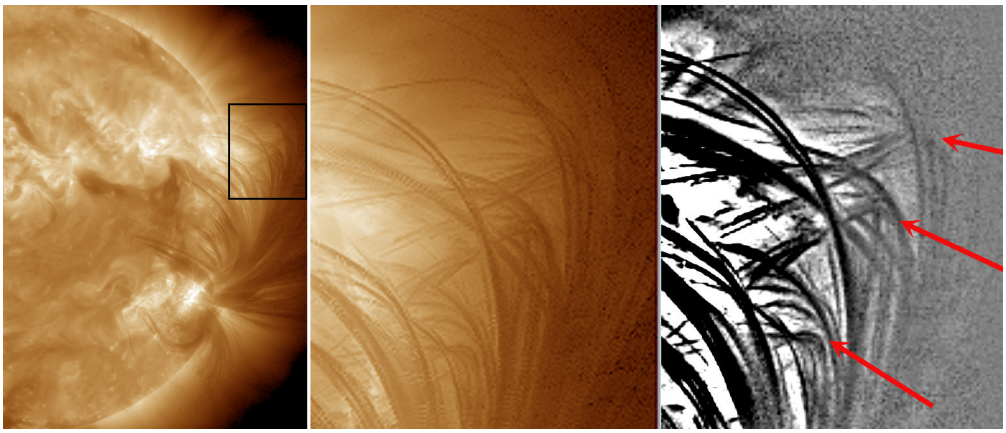

Fig. 10.— A close-up view the trajectories in the persistence map shown in Figure 9. The box in the left panel shows the location of the close-up views in the second panel. The third panel is an enhanced version of the second panel. The red arrows indicate sharp bends in the trajectory of some pieces of prominence, which contrast from the majority of the rest.

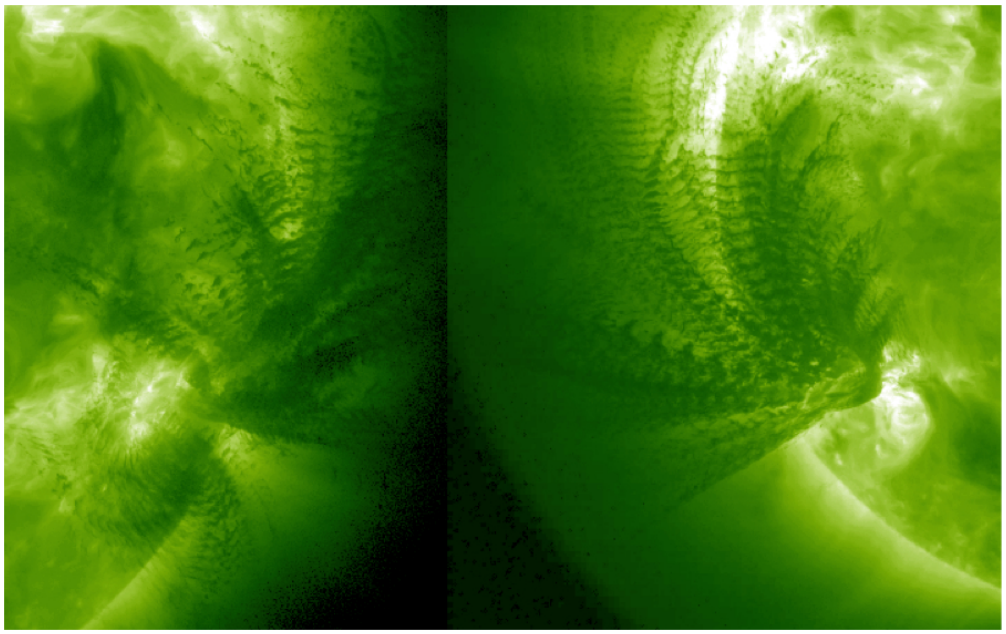

Fig. 11.— Persistence maps of SDO and STEREO-A EUVI images for the fields of view shown in Figure 8, "strobed" at a cadence of 2 minutes, as opposed to the 12-minute cadence in Figure 9.